Proceedings of the 45th ISCIE International Symposium
on Stochastic Systems Theory and Its Applications
Okinawa, Nov. 1-2, 2013

The Effect of Visual Feedback on Coupled Balancing Tasks with Artificial Controllers

Shigeki Matsumoto and Katsutoshi Yoshida
Department of Innovation Systems Engineering, Utsunomiya University,
Yoto 7-1-2, Utsunomiya, Tochigi 321-8585, Japan
E-Mail: matsumoto@katzlab.jp

Abstract

In this paper, we experimentally investigate the cooperative balancing task on a virtual coupled inverted pendula (CIP) model, performed by a pair of an invisible artificial controller and a human subject, where experimental participants were not allowed to watch the movement of the artificial partner during experiments. The experimental result on Lyapunov exponents implies that the human subjects who never have experienced the balancing tasks with visible controller, seems to try to make the artificial controller neutrally stable as well as the subjects who have already experienced. Therefore, the result implies that at least as to the human subjects in the present study, there are no influence of learning with the visible controller on the stabilities of the task with invisible controller.

1 Introduction

Competitive and cooperative dynamics can arise when multiple agents such as humans and robots share common resources and environment [1, 2, 3]. Seeking a simpler mechanical description of such dynamics, we have already proposed the coupled inverted pendula (CIP) model as shown in Fig.1. The CIP model consists of two inverted pendulums independently stabilized whose tips are mechanically linked by a rigid rod [4, 5]. In our recent studies [6, 8], we numerically and experimentally investigated the cooperative balancing dynamics produced by the pair of two artificial controllers and that by the pair of two human subjects, based on the CIP model.

The artificial controller in our studies was composed by a delayed state feedback controller with a randomly fluctuated gain, which was proposed by Cabrera et al. [9, 10]. He showed numerically and experimentally that intermittent behavior typical of the human balancing tasks can precisely be simulated based on the minimally stable design of the controller [9]. In our first study [11], we examined another combination, a pair of the artificial controller and the human subject. Specifically, we experimentally studied how human subjects tune their control properties when playing balancing tasks in cooperation with the given artificial controller having several different specifications, where all participants were able to see movements of the artificial partner as well as their own

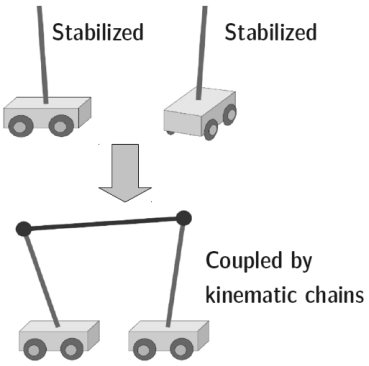

Fig. 1: CIP model.

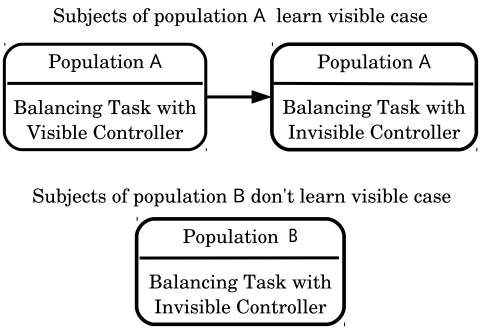

Fig. 2: Concept.

movements. To this end, we developed an experimental system composed by a numerical simulator of the CIP whose control input could be connected with the human manipulation by mice. The experimental result on Lyapunov exponents implied that the human subject seemed to try to make the artificial controller neutrally stable [11].

In our second study [12], we already confirmed the result that the human subject in the invisible case seemed to try to make the artificial controller neutrally stable as well as in the visible case [11]. However, the result might be affected by learning, because the subjects had experienced the balancing tasks with the visible artificial controller.

Therefore, in this paper, we investigate an influence of learning the visible case on the stabilities of invisible case. For this purpose, we consider two types of population A and B as shown in Fig.2, where the subjects in the population A have already experienced the coupled balancing

Table 1: List of state vectors

	Single balance	Coupled balance
Human agent		$\boldsymbol{\Delta X}_H = (\Delta X_H, \Delta \dot{X}_H)^T$ where $\Delta X_H := X^t - U_H$
Artificial agent	$\boldsymbol{\Delta x}_A = (\Delta x_A, \Delta \dot{x}_A)^T$ where $\Delta x_A := x_A^t - u_A$	$\boldsymbol{\Delta X}_A = (\Delta X_A, \Delta \dot{X}_A)^T$ where $\Delta X_A := X^t + l - U_A$
Total System		$\boldsymbol{\Delta X} = (\Delta X_H, \Delta \dot{X}_H, \Delta X_A, \Delta \dot{X}_A)^T$

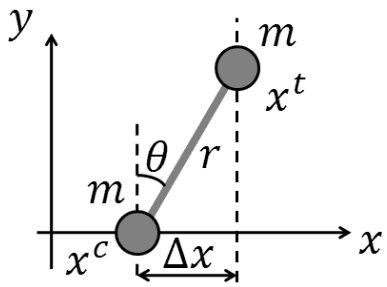

Fig. 3: Inverted pendulum.

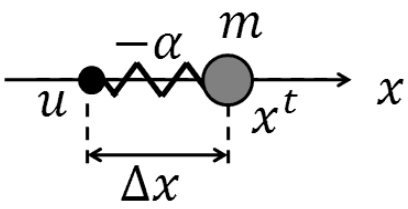

Fig. 4: Linearized inverted pendulum.

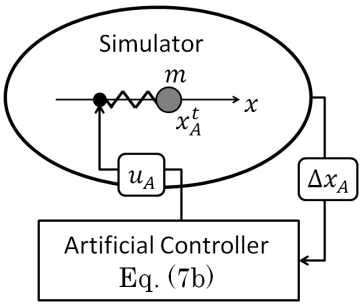

Fig. 5: Single balance control system with an artificial agent.

task with visible controller, while those in the population B never have experienced.

As a result, it will be shown that the subjects of the population B exhibits typical stabilities quite similar to those of the population A. Therefore, the result implies that there are no influence of learning the visible case.

2 Single artificial balance

Firstly, we provide the basic mechanism of the single balance with the artificial controller used in this paper.

We consider an inverted pendulum model as shown in Fig.3, where g is gravity, m is mass, r is length of the stick, θ is a slant angle, and x^t and x^c are absolute positions of the upper and lower end of the stick. The equations of motion are given by

$$\begin{cases} 2m\ddot{x}^c + mr(\cos\theta)\ddot{\theta} - mr\dot{\theta}^2 \sin\theta = 0, \\ mr(\cos\theta)\ddot{x}^c + mr^2\ddot{\theta} - mgr\sin\theta = 0. \end{cases} \tag{1}$$

In the following, we refer to the upper and lower end of the stick as the target and cart respectively.

For simplicity, assuming

$$|\theta| \ll 1, \quad |\dot{\theta}| \ll 1, \tag{2}$$

we obtain a linearized equations of (1),

$$\begin{cases} \ddot{x}^c + g\theta = 0, \\ r\ddot{\theta} - 2g\theta = 0, \end{cases} \tag{3}$$

where the angular displacement and acceleration, θ and $\ddot{\theta}$, can be rewritten using trigonometry as

$$\theta \approx \frac{1}{r}(x^t - x^c), \quad \ddot{\theta} \approx \frac{1}{r}(\ddot{x}^t - \ddot{x}^c). \tag{4}$$

Substituting (4) into (3), we obtain

$$\begin{cases} \ddot{x}^t - \frac{g}{r}(x^t - x^c) = 0, \\ \ddot{x}^c + \frac{g}{r}(x^t - x^c) = 0. \end{cases} \tag{5}$$

.

In this paper, adding viscous damping terms into (5), we consider the following model:

$$\begin{cases} \ddot{x}^t + \gamma\dot{x}^t - \alpha(x^t - x^c) = 0, \\ \ddot{x}^c + \gamma\dot{x}^c + \alpha(x^t - x^c) = 0, \end{cases} \tag{6}$$

where γ is viscous damping coefficient and $\alpha = g/r$.

Secondly, we introduce the control system of the linearized inverted pendulum model (6) as shown in Fig.4, where the motion of the cart x^c is inputted by external displacement u. A black point in Fig.4 represents the position of the cart whose mass is $m = 0$.

It is noteworthy that replacing a part of the dynamical system with external displacement can often be found in common general textbooks such as Landau and Lifshitz [13].

In the single artificial balance, the input u is defined as the output of the artificial controller, $u = u_A$, as shown in Fig.5. In this paper, we consider the artificial controller

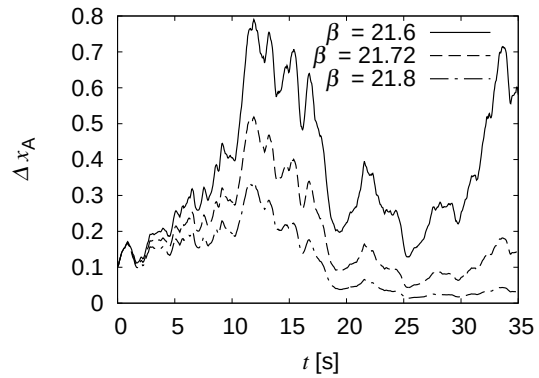

Fig. 6: Sample paths of the balancing error $\Delta x_A(t)$.

proposed by Cabrera [9, 10] that can be given in the following form:

$$\ddot{x}^t(t) + \gamma \dot{x}^t(t) - \alpha(x^t(t) - u_A(t)) = 0, \tag{7a}$$

$$\ddot{u}_A(t) + \gamma \dot{u}_A(t) - R(t)(x^t(t-\tau) - u_A(t-\tau)) = 0, \tag{7b}$$

where τ is a time delay representing the latency of neural reflexes in human balancing tasks and $R(t) = \beta(1 + \nu w(t))$ is a random feedback gain, $w(t)$ is standard Gaussian white noise, and ν represents the strength of the noise.

Using the balancing error defined by $\Delta x_A := x^t - u(t)$, we can rewrite (7) as

$$\Delta\ddot{x}_A(t) + \gamma\Delta\ddot{x}_A(t) - \alpha\Delta x_A(t) + R(t)\Delta x_A(t-\tau) = 0. \tag{8}$$

For convenience of reference, Table 1 lists the notation of state vectors used in this paper including Δx_A, x_A^t and u_A above. That is, the lower case and upper case of vectors represent the single and coupled balance respectively, and subscripts H and A represent the human and artificial agents respectively. In this way, the vector $\boldsymbol{\Delta x_A}$ in Table 1 represents that of single artificial balance, and the vectors $\boldsymbol{\Delta X}_H$ and $\boldsymbol{\Delta X}_A$ represent those of the human part and the artificial part of the coupled balance respectively, and the state vector $\boldsymbol{\Delta X}$ consists of the vector elements of $\boldsymbol{\Delta X}_H$ and $\boldsymbol{\Delta X}_A$.

We now numerically calculate the solution of the system (7). In the following, we assume $\gamma = 6$, $\alpha = 22$, $\nu = 2$ and $\tau = 0.1$ and set initial values of the model to $[x_A^t, \dot{x}_A^t, u_A, \dot{u}_A] = [0.1, 0, 0, 0]$. This means that the initial values of balancing error are set to $[\Delta x_A, \Delta\dot{x}_A] = [0.1, 0]$. The target x_A^t is repelled from the cart u_A by a linear spring with a negative coefficient $-\alpha < 0$ that simulates the gravity force in the original inverted pendulum. For numerical integrations of (7), a fourth-order Runge-Kutta-Gill method is employed with the time step 1×10^{-3}s.

Fig.6 shows sample paths obtained from (7) subjected to a common sample of the noise $w(t)$. It appears that the state $\Delta x_A(t)$ diverges for the gain $\beta = 21.6$ and converges for the gain $\beta = 21.8$. On the other hand, near half point $\beta = 21.72$, the bounded state dose not converge nor diverge.

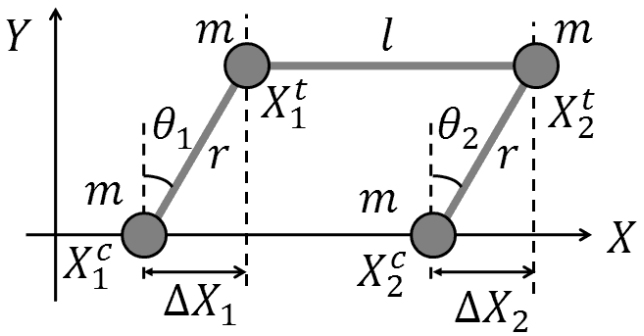

Fig. 7: Coupled inverted pendulum.

Therefore, not surprisingly, it is confirmed that stabilities of the single balance control system with an artificial controller directly depend on the feedback gain β.

3 Coupled balancing tasks

The main interest of this paper is coupled balancing task between the human and artificial agents.

For this purpose, we consider a CIP model as shown in Fig.7 in which tips of two inverted pendulums in Fig.3 are linked by a connection rod, where θ_i is angle of ith pendulum, and X_i^t and X_i^c are absolute positions of the target and the cart of the ith pendulum.

The equations of motion of the CIP model in Fig.7 is given in the following form:

$$\begin{cases} 2m\ddot{X}_1^c + mr(\cos\theta_1)\ddot{\theta}_1 - mr\dot{\theta}_1^{\,2}\sin\theta_1 - \lambda\frac{d\phi}{dX_1^c} = 0, \\ mr(\cos\theta_1)\ddot{X}_1^c + mr^2\ddot{\theta}_1 - mgr\sin\theta_1 - \lambda\frac{d\phi}{d\theta_1} = 0, \\ 2m\ddot{X}_2^c + mr(\cos\theta_2)\ddot{\theta}_2 - mr\dot{\theta}_2^{\,2}\sin\theta_2 - \lambda\frac{d\phi}{dX_2^c} = 0, \\ mr(\cos\theta_2)\ddot{X}_2^c + mr^2\ddot{\theta}_2 - mgr\sin\theta_2 - \lambda\frac{d\phi}{d\theta_2} = 0, \end{cases} \tag{9}$$

where λ is undetermined multiplier and ϕ is a constraint condition of the rod as follows,

$$\phi := (r\sin\theta_1 - r\sin\theta_2 + X_1^c - X_2^c)^2 + (r\cos\theta_1 - r\cos\theta_2)^2 - l^2 = 0. \tag{10}$$

Assuming

$$|\theta_i| \ll 1, \qquad |\ddot{\theta}_i| \ll 1, \tag{11}$$

we obtain linearized equations of (9),

$$\begin{cases} 2m\ddot{X}_1^c + mr\ddot{\theta}_1 - \lambda\frac{d\phi}{dX_1^c} = 0, \\ mr\ddot{X}_1^c + mr^2\ddot{\theta}_1 - mgr\theta_1 - \lambda\frac{d\phi}{d\theta_1} = 0, \\ 2m\ddot{X}_2^c + mr\ddot{\theta}_2 - \lambda\frac{d\phi}{dX_2^c} = 0, \\ mr\ddot{X}_2^c + mr^2\ddot{\theta}_2 - mgr\theta_2 - \lambda\frac{d\phi}{d\theta_2} = 0, \end{cases} \tag{12}$$

and a linearized form of (10),

$$\phi = (r\theta_1 - r\theta_2 + X_1^c - X_2^c)^2 - l^2 = 0, \tag{13}$$

with the derivatives,

$$\begin{cases} \frac{d\phi}{dX_1^c} = 2((X_1^c - X_2^c) + r(\theta_1 - \theta_2)), \\ \frac{d\phi}{d\theta_1} = 2r((X_1^c - X_2^c) + r(\theta_1 - \theta_2)), \\ \frac{d\phi}{dX_2^c} = -2((X_1^c - X_2^c) + r(\theta_1 - \theta_2)), \\ \frac{d\phi}{d\theta_2} = -2r((X_1^c - X_2^c) + r(\theta_1 - \theta_2)). \end{cases} \tag{14}$$

Subtracting fourth equation from second equation in (12), we obtain

$$\begin{aligned} mr(\ddot{X}_1^c - \ddot{X}_2^c + r\ddot{\theta}_1 - r\ddot{\theta}_2) - mgr(\theta_1 - \theta_2) \\ - 4r\lambda(X_1^c - X_2^c + r\theta_1 - r\theta_2) = 0. \end{aligned} \tag{15}$$

Then, substituting a reduced form of (13),

$$X_1^c - X_2^c = l - r\theta_1 + r\theta_2 \tag{16}$$

and the second order derivative of (16),

$$\ddot{X}_1^c - \ddot{X}_2^c = \ddot{l} - r\ddot{\theta}_1 + r\ddot{\theta}_2, \tag{17}$$

into (15), we obtain

$$mr\ddot{l} - 4lr\lambda - mgr(\theta_1 - \theta_2) = 0. \tag{18}$$

Since $\phi = 0$ in (13) implies $\ddot{\phi} = 0$ and $l \neq 0$, we have $\ddot{l} = 0$ from

$$\begin{aligned} \ddot{\phi} &= 2l(\ddot{X}_1^c - \ddot{X}_2^c + r\ddot{\theta}_1 - r\ddot{\theta}_2) \\ &= 2l\ddot{l} = 0. \end{aligned} \tag{19}$$

From the above, we have the solution of (18) in λ,

$$\lambda = \frac{-mg(\theta_1 - \theta_2)}{4l}. \tag{20}$$

Substituting (14) and (20) into (12), we obtain

$$\begin{cases} \ddot{X}_1^c + g\theta_1 = 0, \\ \ddot{\theta}_1 - \frac{gm(3\theta_1 + \theta_2)}{2mr} = 0, \\ \ddot{X}_2^c + g\theta_2 = 0, \\ \ddot{\theta}_2 - \frac{gm(\theta_1 + 3\theta_2)}{2mr} = 0. \end{cases} \tag{21}$$

Since we have assumed $|\theta_i| \ll 1$, the angular displacements θ_i and accelerations $\ddot{\theta}_i$ can be rewritten using trigonometry as

$$\begin{cases} \theta_1 \approx \frac{X_1^t - X_1^c}{r}, \\ \theta_2 \approx \frac{X_2^t - X_2^c}{r}, \\ \ddot{\theta}_1 \approx \frac{\ddot{X}_1^t - \ddot{X}_1^c}{r}, \\ \ddot{\theta}_2 \approx \frac{\ddot{X}_2^t - \ddot{X}_2^c}{r}, \end{cases} \tag{22}$$

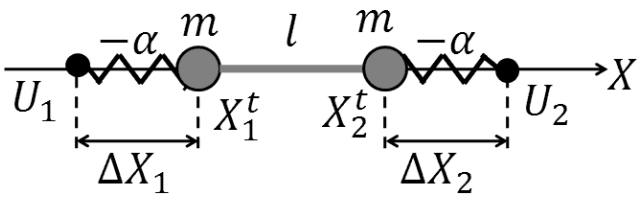

Fig. 8: Linearized coupled inverted pendulum.

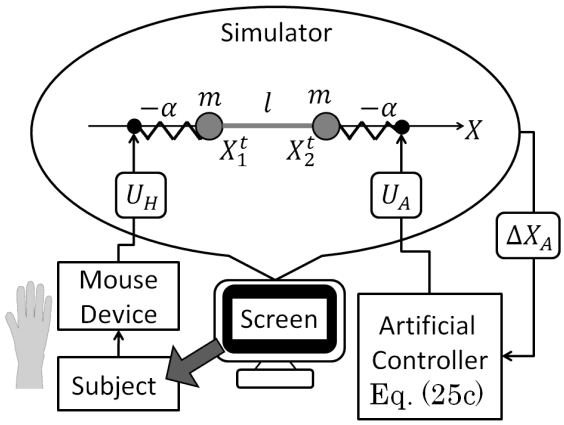

Fig. 9: Coupled balance control system with the human subject and the artificial controller.

where $X_2^t = X_1^t + l$.

Substituting (22) into (21), we have a linearized version of the nonlinear CIP model, in (9) as

$$\begin{cases} \ddot{X}_i^t + \frac{g}{2r}(X_1^t - X_1^c + X_1^t - X_2^c + l) = 0, \\ \ddot{X}_i^c + \frac{g}{r}(X_i^t - X_i^c) = 0. \qquad (i = 1, 2) \end{cases} \tag{23}$$

In this paper, adding viscous damping terms into (23), we consider the following form:

$$\ddot{X}^t + \gamma\dot{X}^t + \frac{\alpha}{2}(2X^t - X_1^c - X_2^c + l) = 0, \tag{24a}$$

$$\ddot{X}_i^c + \gamma\dot{X}^t + \alpha(X_i^t - X_i^c) = 0, \qquad (i = 1, 2) \tag{24b}$$

where $\alpha = g/r$, $X^t = X_1^t$, $\dot{X}^t = \dot{X}_1^t = \dot{X}_2^t$.

Next, we introduce the control system of CIP model as shown in Fig.8, where the motion of the carts X_i^c are inputted by external displacements U_i. Two black points in Fig.8 represent the position of the carts. In this coupled balance, the input U_1 is defined as human manipulation U_H and input U_2 as the output of the artificial controller U_A.

Now we design the experimental system of coupled balance between human and artificial agent as shown in Fig.9, that consists of a computer with the numerical simulator of linearized CIP model in Fig.8, a mouse device and a display. The simulator calculates the dynamics of positions of the targets X^t, and the carts U_H, U_A, and velocities of the targets $\dot{X}^t$, and the carts $\dot{U}_A$, $\dot{U}_H$, and the balancing errors ΔX_H, ΔX_A, defined in Table 1.

Solving (25) below, the simulator creates animation of the model to display on the screen. The mouse, manipulated by human subject, inputs the position of the cart U_H into the simulator.

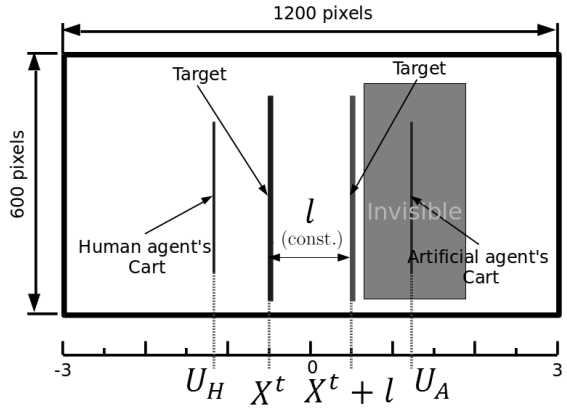

Fig. 10: Screen design of the coupled balance control system.

Thus, the governing equations of the simulator are given in following form:

$$\ddot{X}^t(t) + \gamma \dot{X}^t(t) + \frac{\alpha}{2}(2X^t(t) - U_H(t) - U_A(t) + l) = 0, \quad (25a)$$

$$U_H(t) := (\text{manipulation by a human subject}), \quad (25b)$$

$$\ddot{U}_A(t) + \gamma \dot{U}_2(t) - R(t)(X^t(t-\tau) - U_A(t-\tau) + l) = 0, \quad (25c)$$

where (25a) comes from (24a), and (25c) is the same as (7b).

In the following, we select parameters of (25) as $\gamma = 6$, $\alpha = 22$, $l = 1$, $\nu = 2$ and $\tau = 0.1$, the same values as in our previous study [11]. The initial values of the model are set to $[X^t, \dot{X}^t, U_H, \dot{U}_H, U_A, \dot{U}_A] = [-0.5, 0, -0.6, 0, 0.6, 0]$. This means that the initial balancing errors, are set to $[\Delta X_H, \Delta X_A] = [0.1, -0.1]$. The movement performed by subject U_H is measured and substituted into the numerical model (25) with the sampling rate of 20Hz, while the balancing image on the screen is animated at the same rate.

The screen design of coupled balance control system is shown in Fig.10. The thick lines represent the targets X^t and $X^t + \ell$, while the thin lines represent the carts U_A and U_H. In our previous study, in the experiment of visible case, all of the four lines (two thick and two thin lines) were displayed [11]. On the contrary, in the experiment of invisible case, a thin line in the right-hand side, which is assigned to the artificial agent, is not displayed. It follows that the human subject can not see movements of the artificial partner.

Following this setup, we conduct the experiment to measure the time series of X^t, U_H and U_A in (25), for the population A and B in the invisible case.

3.1 Experimental condition for the population A

Subjects of A are ten healthy males in their early twenties. The subjects performed and learned the coupled balance of visible case before measurement of the invisible case. In both the visible and invisible cases, the subjects were first instructed how to operate the measurement system, the number of trials to be performed, the initial configuration of the target model, and the time interval of trials.

First, in the visible case, they began the operation upon hearing a signal and attempted to maintain the balance for 60 seconds. If the targets or carts left the screen in less than 60 seconds, the trial was repeated. After the 10 trials, the value of feedback gain β is updated to be less from 23 to 17 at regular intervals. After completing the 40 trials, learning was over.

Next, in the invisible case, we conducted measurements for the population A. The number of trials to be performed, the time interval of trial and the way of updating feedback gain β are the same as the visible case above.

3.2 Experimental condition for the population B

Subjects for B are ten healthy males different from those for A in their early twenties. The subjects performed the coupled balancing task of invisible case without experience of visible case. They were first instructed the same instruction as in the section 3.1. Then, the number of trials to be performed, the time interval of trial and the way of updating feedback gain β were the same as in the section 3.1, again.

3.3 Experimental data

We show here the experimental data of the time series of the balancing task for the population B in the invisible case. Note that the experimental data of A in the invisible case have already been shown in our previous study [12].

Fig.11 and Fig.12 show typical time series of the balancing errors for $\beta = 23$ and for $\beta = 17$ respectively. The solid line represents a balancing error of the human subject ΔX_H and the dashed line represents that of the artificial controller ΔX_A.

In contrast to the single artificial balancing shown in Fig.6 where the stability of $\Delta x_A(t)$ depends on the feedback gain β, it seems that no significant dependency on β can be found for the coupled balance shown in Fig.11 and Fig.12. That is, it seems that there is no significant change of stability of ΔX_H and ΔX_A around $\Delta X = 0$ between the different conditions $\beta = 23$ and $\beta = 17$.

4 Stability of coupled balancing tasks

In order to evaluate stabilities of the balancing errors, we employ Lyapunov exponents as follows.

4.1 Lyapunov exponents

Consider an n-dimensional dynamical system:

$$\dot{\boldsymbol{x}}(t) = \boldsymbol{f}\big(\boldsymbol{x}(t)\big) \quad \boldsymbol{x}(0) = \boldsymbol{x}_0 \quad (26)$$

and its linearized system:

$$\dot{\boldsymbol{\xi}}(t) = J\big(\boldsymbol{x}(t)\big)\boldsymbol{\xi}(t), \quad \boldsymbol{\xi}(0) = \boldsymbol{\xi}_0 \quad (27)$$

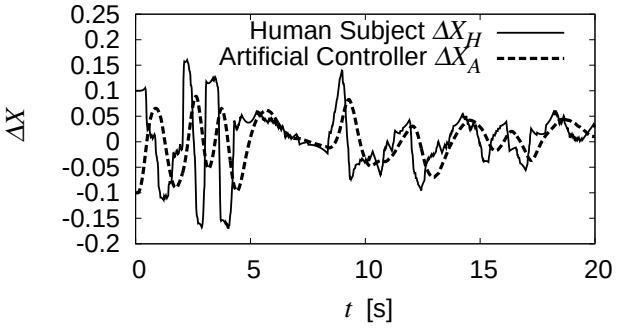

Fig. 11: Balancing error ΔX_H and ΔX_A for $\beta = 23$

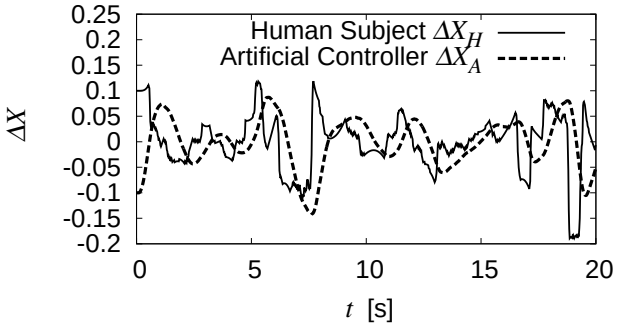

Fig. 12: Balancing error ΔX_H and ΔX_A for $\beta = 17$

where $J(\boldsymbol{x}) = \partial \boldsymbol{f}/\partial \boldsymbol{x}$ is the Jacobian matrix of $\boldsymbol{f}$ along the trajectory $\boldsymbol{x}(t)$. Then, the largest Lyapunov exponent (LLE) of the dynamical system (26) is defined by

$$\lambda(\boldsymbol{x}) = \max_{\boldsymbol{\xi}_0} \lim_{t\to\infty} \frac{1}{t} \ln \frac{\|\boldsymbol{\xi}(t)\|}{\|\boldsymbol{\xi}(0)\|} \tag{28}$$

where $\|\cdots\|$ is a norm of vectors. In general, the orbit $\boldsymbol{x}(t)$ is stable for $\lambda < 0$, unstable for $\lambda > 0$, and neutrally stable for $\lambda = 0$.

When the system equation (26) is explicitly known, one can calculate the LLE $\lambda(\boldsymbol{x})$ by solving (27) along with (26) numerically.

On the contrary, another approach is required for the balance control systems including human agents because their system equation is not explicitly known. For this purpose, we employ an effective method of estimating the LLE from physical time series proposed by Sano and Sawada [14]. In this case, a time series $\boldsymbol{x}_j = \boldsymbol{x}\big(t_0 + (j-1)\Delta t\big)$ of the target system is assumed to be known where Δt is a sampling time of measurement. Then, consider a small ball of radius ϵ centred at the orbit point $\boldsymbol{x}_j$ and find any set of N points $\{\boldsymbol{x}_{k_i}\}_{i=1}^N$ included in this ball and define the displacement vectors:

$$\boldsymbol{y}^i := \boldsymbol{x}_{k_i} - \boldsymbol{x}_j, \quad (i = 1, 2, \cdots, N). \tag{29}$$

After the evolution of a time interval $m\Delta t$, the orbital point $\boldsymbol{x}_j$ will proceed to $\boldsymbol{x}_{k_i+m}$ and neighboring points $\{\boldsymbol{x}_{k_i}\}_{i=1}^N$ to $\{\boldsymbol{x}_{k_i+m}\}_{i=1}^N$. The displacement vector $\boldsymbol{y}^i$ is thereby mapped to

$$\boldsymbol{z}^i := \boldsymbol{x}_{k_i+m} - \boldsymbol{x}_{j+m}, \quad (i = 1, 2, \cdots, N). \tag{30}$$

If the radius ϵ is sufficiently small, the evolution of $\boldsymbol{y}^i$ to $\boldsymbol{z}^i$ can be represented by

$$\begin{cases} \boldsymbol{z}^i = A_j \boldsymbol{y}^i, \\ A_j V = C, \\ (V)_{kl} = \frac{1}{N}\sum_{i=1}^N (\boldsymbol{y}^i)_k (\boldsymbol{y}^i)_l^T, \\ (C)_{kl} = \frac{1}{N}\sum_{i=1}^N (\boldsymbol{z}^i)_k (\boldsymbol{y}^i)_l^T, \end{cases} \tag{31}$$

where $(\cdots)_k$, $(\cdots)_{kl}$ denotes the k component of vector and the (k,l) component of matrix respectively. Finally, using the estimated matrix A_j in (31), we can define the LLE of the time series $\boldsymbol{x}_j$ as

$$\lambda(\boldsymbol{x}_j) = \max_{\boldsymbol{e}} \lim_{n\to\infty} \frac{1}{n\Delta t} \sum_{j=1}^{n} \ln \frac{\|A_j \boldsymbol{e}\|}{\|\boldsymbol{e}\|} \tag{32}$$

where $\boldsymbol{e}$ is tangent vector at $\boldsymbol{x}_j$.

Table 2: LLEs for the population A and B.

Population	LLEs
A	$\lambda_\beta^{\mathsf{A}}$
B	$\lambda_\beta^{\mathsf{B}}$

In this way, we can obtain the LLE such as $\lambda(\Delta \boldsymbol{X})$ of the total dynamics of coupled balance between human and artificial agents for both the population A and B.

In the same way, it is also possible to obtain the sub-LLE of the human part $\lambda(\Delta \boldsymbol{X}_H)$, the artificial part $\lambda(\Delta \boldsymbol{X}_A)$ of the coupled balance for both the population A and B. For convenience of reference, Table 2 lists the LLEs used in this paper. That is, subscripts A and B represent the populations A and B respectively.

Although one can calculate the LLE of single balance with a artificial agent $\lambda(\Delta \boldsymbol{x}_A)$ by solving (27) along with (8) generally, in what follows, we calculate it from physical time series to equalize calculation processes of the LLE and sub-LLE. In the following, we choose $\epsilon = 0.05$, $N = 10$ and $m = 200$.

4.2 LLE of the total dynamics

The mean values of all LLEs are shown in Fig.13, and those with 95% confidence intervals are shown in Fig.14.

The white and black squares in Fig.13 represent the mean LLEs of the total dynamics of coupled balance, $\overline{\lambda_\beta^{\mathsf{A}}}(\Delta \boldsymbol{X})$ for the population A and $\overline{\lambda_\beta^{\mathsf{B}}}(\Delta \boldsymbol{X})$ for the population B respectively, and the cross marks in Fig.13 represent LLEs, $\lambda_\beta(\boldsymbol{\Delta x_A})$, of the single artificial balance as functions of the feedback gain β. The error bars plotted

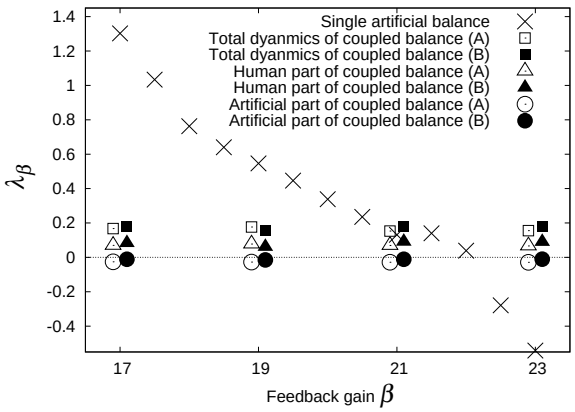

Fig. 13: Mean LLEs of the experiments.

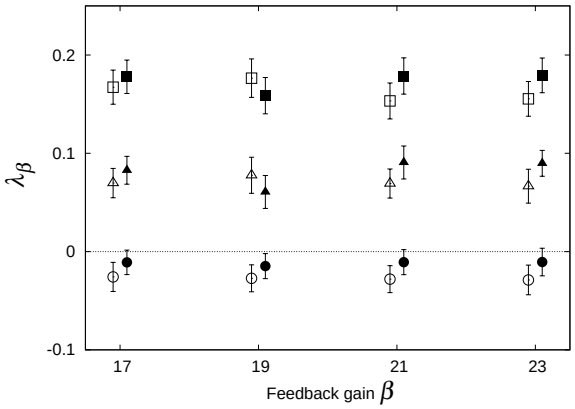

Fig. 14: Mean LLEs of the experiments with 95% confidence intervals.

along with the white and black squares in Fig.14 represent 95% confidence intervals of the mean values $\overline{\lambda_\beta^{\mathsf{A}}}(\Delta \boldsymbol{X})$ and $\overline{\lambda_\beta^{\mathsf{B}}}(\Delta \boldsymbol{X})$ respectively.

Since $\lambda_\beta(\Delta \boldsymbol{x}_A)$ in Fig.13 is a monotonically decreasing function of β, it is clear that the stability of the single artificial balancing depends on the feedback gain β as was also commented in Fig.6. In contrast, it appears in Fig.13 and Fig.14 that both $\overline{\lambda_\beta^{\mathsf{A}}}(\Delta \boldsymbol{X})$ and $\overline{\lambda_\beta^{\mathsf{B}}}(\Delta \boldsymbol{X})$ take nearly constant positive values around $\lambda_\beta \approx 0.15 > 0$ for any β. This means that the total dynamics of coupled balance for both the population A and B, exhibit nearly constant instability independently of existence of coupling and of the feedback gain of the artificial part.

As for the coupled balance, since β represents the feedback gain of the artificial part, not of the human part, the result implies that the nearly constant instability of the coupled balance found in Fig.13 and Fig.14 is possibly produced by the human part. In other words, it seems that the human part may adjust itself to make the total stability of the coupled balance nearly constant. This feature can also be found in Fig.11 and Fig.12 where the different values of β does not cause big changes in the time responses of the coupled balance.

4.3 Sub-LLEs of the human part

The white and black triangles in Fig.13 represent the mean sub-LLEs of the human part of the coupled balance, $\overline{\lambda_\beta^{\mathsf{A}}}(\Delta \boldsymbol{X}_H)$ for the population A and $\overline{\lambda_\beta^{\mathsf{B}}}(\Delta \boldsymbol{X}_H)$ for the population B respectively as functions of the feedback gain β.

The error bars plotted along with the white and black triangles in Fig.14 represent 95% confidence intervals of the mean values $\overline{\lambda_\beta^{\mathsf{A}}}(\Delta \boldsymbol{X}_H)$ and $\overline{\lambda_\beta^{\mathsf{B}}}(\Delta \boldsymbol{X}_H)$ respectively.

It appears in Fig.13 and Fig.14 that both $\overline{\lambda_\beta^{\mathsf{A}}}(\Delta \boldsymbol{X}_H)$ and $\overline{\lambda_\beta^{\mathsf{B}}}(\Delta \boldsymbol{X}_H)$ take nearly constant positive values around $\lambda_\beta \approx 0.08 > 0$. This means that the human part in the coupled balance always exhibits nearly constant instability with β for both the population A and B.

4.4 Sub-LLEs of the artificial part

The white and black circles in Fig.13 represent the mean sub-LLEs of the artificial part of coupled balance, $\overline{\lambda_\beta^{\mathsf{A}}}(\Delta \boldsymbol{X}_A)$ for the population A and $\overline{\lambda_\beta^{\mathsf{B}}}(\Delta \boldsymbol{X}_A)$ for the population B respectively. The error bars plotted along with the white and black circles in Fig.14 represent 95% confidence intervals of the mean values $\overline{\lambda_\beta^{\mathsf{A}}}(\Delta \boldsymbol{X}_A)$ and $\overline{\lambda_\beta^{\mathsf{B}}}(\Delta \boldsymbol{X}_A)$ respectively.

It is clear from the result on $\overline{\lambda_\beta^{\mathsf{A}}}(\Delta \boldsymbol{X}_A)$ and $\overline{\lambda_\beta^{\mathsf{B}}}(\Delta \boldsymbol{X}_A)$ in Fig.13 and Fig.14 that the artificial part of the coupled balance between the human subject and the artificial partner, maintains nearly a constant small negative value close to 0 of the LLE. This means that artificial part in the coupled balance exhibits nearly constant neutrally stable with β for both the population A and B. The above result implies that at least as to the human subjects in the present study, there are no influence of learning the visible case on the stabilities of invisible case. It follows that the property of human, seeking the neutrally stable artificial partners, tends to be so fundamental as to arises in the invisible case without the experience of the visible case.

5 Conclusion

We have investigated an influence of learning the dynamics in the visible case on the stabilities of the dynamics in the invisible case. For this purpose, we consider two types of population A and B, where the subjects in the population A have already experienced the balancing task with visible controller, while those in the population B never have experienced.

To this end, in both cases of the population A and B, we conducted the experiment to measure the time responses of the balancing errors in the coupled balance between the human subjects and the invisible artificial controller, where the visual information of the artificial controller is not given to the human subjects. We then calculated the largest Lyapunov exponent (LLE) of the balancing errors in order to evaluate their stabilities and obtained the following results.

1. The stability of the single artificial balance monotonically depends on the feedback gain β.

2. In contrast, the total dynamics of the coupled balance between the human and artificial agents exhibits instability nearly constant with β for both the population A and B. It follows that stabilities of the total dynamics of coupled balance for the population B is quite similar to those for the population A.

3. The human part in the coupled balance always exhibits nearly constant instability with β for both the population A and B. It follows that stabilities of the human part of coupled balance for the population B is quite similar to those for the population A, again.

4. The artificial part in the coupled balance exhibits nearly constant neutrally stable with β for both the population A and B. It follows that stabilities of the artificial part of coupled balance for the population B is quite similar to those for the population A, again.

From the above result, it can be concluded that at least as to the human subjects in the present study, there are no influence of learning the visible case on the stabilities of the invisible case. This implies that the property of human, seeking the neutrally stable artificial partners, appears to be so fundamental as to arises in the invisible case without the experience of the visible case.

In future work, the dynamical property described above is expected to provide a new criterion for designing human-like motions of artificial agents such as human-like partner robots because the property of human described above, seeking the neutrally stable artificial partners, seems to be hardly obtainable from the conventional design principles of control systems engineering.

Acknowledgement

We wish to express our gratitude to the students of Utsunomiya University for their participation and cooperation as subjects in this study.

References

[1] Osumi, H., Arai, T., Yoshida, N., Shen, Y., Asama, H., Kaetsu, H., and Endo, I., Cooperative System between a Position-controlled Robot and a Crane with Three Wires, *Distributed Autonomous Robotic Systems*, Springer-Verlag, Vol.1, pp.347-358, 1994.

[2] Hirata, Y., Kosuge, K., Asama, H., Kaetsu, H., and Kawabata, K., Handling of a Large Object using Multiple Mobile Robots in Coordination, *Trans. JSME, Series C*, Vol.67, No.656, pp.1077-1084, 2001. (in Japanese)

[3] Sigmund, K., and Hofbauer, J., *Evolutionary Games and Population Dynamics*, Cambridge University Press, 1998.

[4] Yoshida, K., Yokota, K., and Watanabe, S., A Study on Mechanical System Representation of Competition and Cooperation, *Trans. JSME, Series C*, Vol.74, No.741, pp.1311-1316, 2008. (in Japanese)

[5] Yoshida, K., and Ohta, H., Coupled Inverted Pendula Model of Competition and Cooperation *Journal of System Design and Dynamics*, Vol.2, No.3, pp.727-737, 2008.

[6] Yoshida, K., Higeta, A., and Watanabe, S., Effects of Mechanical Coupling on the Dynamics of Balancing Tasks, *International Journal of Innovative Computing, Information and Control*, Vol.7, No.4, pp.1661-1674, 2011.

[7] Yoshida, K., Toward Stochastic Explanation of Neutrally Stable Delayed Feedback Model of Human Balance Control. *International Journal of Innovative Computing, Information and Control*, Vol.8, No.3(B), pp.2249-2259, 2012.

[8] Higeta, A., Yoshida, K., Watanabe, S., and Nakatsuka, A., Psychological Measurement of Coupled Human Balancing Tasks. *Proceedings of the 2011 IEEE/SICE International Symposium on System Integration*, pp.661-666, No.C9-3(CD-ROM), 2011.

[9] Cabrera, J. L., and Milton, J. G., On-off Intermittency in a Human Balancing Task. *Physical Review Letters*, Vol.89, No.15, pp.158702:1–4, 2002.

[10] Bormann, R., Cabrera, J. L., J. Milton, G., and Eurich, C. W., Visuomotor Tracking on a Computer Screen an Experimental Paradigm to Study the Dynamics of Motor Control. *Neurocomputing*, Vol.58, No.60, pp.517–523, 2004.

[11] Matsumoto, S., Yoshida, K., and Higeta, A., An Experimental study on Coupled Balancing Tasks between Human Subjects and Artificial Controllers. *Proceedings of The 44th ISCIE International Symposium on Stochastic Systems Theory and Its Applications*, pp. 230–235, 2012.

[12] Matsumoto, S., Yoshida, K., An Experimental Study on Balancing Tasks of Human subjects in Cooperation with Invisible Artificial Partners. *Proceedings of the ASME 2013 Dynamic Systems and Control Conference*, pp.911–919, 2013.

[13] Landau, L. D., Lifshitz, E. M., *Course of Theoretical Physics Volume 1, Mechanics, Second Edition*, Pergamon Press, 1969.

[14] Sano, M., and Sawada, Y., Measurement of the Lyapunov Spectrum from a Chaotic Time Series. *Physical Review Letters*, Vol.55, No.10, pp.1082-1085, 1985.